



This discussion paper is/has been under review for the journal Atmospheric Chemistry and Physics (ACP). Please refer to the corresponding final paper in ACP if available.

# Simultaneous Retrievals of Polar Mesospheric Clouds (PMCs) with Ozone from OMI UV measurements

J. Bak<sup>1</sup>, X. Liu<sup>2</sup>, J. H. Kim<sup>1</sup>, M. T. Deland<sup>3</sup>, and K. Chance<sup>2</sup>

<sup>1</sup>Pusan National University, Department of Atmospheric Sciences, Busan, South Korea

<sup>2</sup>Harvard-Smithsonian Center for Astrophysics, Cambridge, MA, USA

<sup>3</sup>Systems and Applications, Inc. (SSAI), 10210 Greenbelt Rd., Suite 600, Lanham, MD 20706, USA

Received: 1 September 2015 – Accepted: 5 September 2015 – Published: 24 September 2015

Correspondence to: J. H. Kim (jaekim@pusan.ac.kr) and J. Bak (sunnypark@pusan.ac.kr)

Published by Copernicus Publications on behalf of the European Geosciences Union.

Title Page

Abstract

Introduction

Conclusions

References

Tables

Figures



Back

Close

Full Screen / Esc

Printer-friendly Version

Interactive Discussion



## Abstract

The presence of polar mesospheric clouds (PMCs) at high latitudes could affect the retrieval of ozone profiles using backscattered ultraviolet (BUV) measurements. PMC-induced errors in ozone profile retrievals from Ozone Monitoring Instrument (OMI) BUV measurements are investigated through comparisons with Microwave Limb Sounder (MLS) ozone measurements. This comparison demonstrates that the presence of PMCs leads to systematic biases at altitudes above 6 hPa in summer high latitudes; the biases increase from  $\sim -2\%$  at 2 hPa to  $\sim -20\%$  at 0.5 hPa on average, and are significantly correlated with brightness of PMCs. Sensitivity studies show that the radiance sensitivity to PMCs strongly depends on wavelengths, increasing by a factor of  $\sim 4$  from 300 to 265 nm. It also strongly depends on the PMC scattering, thus depending on viewing geometry. The optimal estimation-based retrieval sensitivity analysis shows that PMCs located at 80–85 km have the greatest effect on ozone retrievals at  $\sim 0.2$  hPa ( $\sim 60$  km), where the retrieval errors range from  $-2.5\%$  with PMC optical depth (POD) of  $10^{-4}$  to  $-20\%$  with  $10^{-3}$  at back scattering angles, and the impacts increase by a factor of  $\sim 5$  at forward scattering angles due to stronger PMC sensitivities. To reduce the interference of PMCs on ozone retrievals, we perform simultaneous retrievals of POD and ozone with a loose constraint of  $10^{-3}$  for POD, which results in retrieval errors of  $1-4 \times 10^{-4}$ . It is demonstrated that the negative bias of OMI ozone retrievals relative to MLS could be improved by including the PMC in the forward model calculation and retrieval.

## 1 Introduction

PMCs are tenuous layers of ice crystals that form at 80–85 km altitude only during the hemispheric summer season ( $\sim 30$  days before to  $\sim 65$  days after summer solstice) at high latitudes and occasionally at mid-latitudes (Thomas et al., 1991; Taylor et al., 2002; DeLand et al., 2010). It has been suggested that the change of PMC properties

ACPD

15, 25907–25932, 2015

## Simultaneous Retrievals of PMCs

J. Bak et al.

Title Page

Abstract

Introduction

Conclusions

References

Tables

Figures



Back

Close

Full Screen / Esc

Printer-friendly Version

Interactive Discussion



such as frequency and brightness is linked to long-term changes in the composition and thermal structure of our atmosphere caused by human activities.

The optimal way to observe PMC from space is at the atmospheric limb, where the atmospheric background scattering is very small and the clouds are observed “edge-on” because the limb intensity is about 100 times that of nadir viewing (Thomas et al., 1991). Nevertheless, Thomas et al. (1991) first demonstrated that PMCs are detectable in nadir-looking UV measurements using a brightness-based detection algorithm. PMC occurrence and residual albedo have been derived from Solar Backscatter Ultraviolet (SBUV, SBUV/2) and OMI measurements at shorter wavelengths below 300 nm where the Rayleigh-scattered background is comparatively low due to very strong ozone absorption. Thomas et al. (1991) found an anti-correlation of the PMC occurrence frequency with solar activity from 8 years of SBUV albedo data over the period 1978 to 1986 and demonstrated that the existence of PMCs could affect SBUV ozone profile retrievals with negative biases of  $\sim 10\%$  above 48 km on individual retrievals. Further studies have demonstrated long-term trends over 30+ years in PMC occurrence frequency, albedo, and ice water content (DeLand et al., 2003, 2007; Shettle et al., 2009; DeLand and Thomas, 2015). Therefore, failure to account for PMCs in ozone retrievals might affect the determination of ozone trends in the upper stratosphere.

This paper is motivated by two main goals. The first objective is to examine the impact of PMCs on OMI ozone profile retrievals. For this purpose, we combine the OMI PMC detection algorithm of DeLand et al. (2010) and the OMI ozone profile retrieval algorithm of Liu et al. (2010a) and evaluate OMI ozone profiles for PMC and non-PMC pixels through comparison with collocated MLS measurements. The second one is to simultaneously retrieve PMC optical depth with ozone using optimal estimation technique, to reduce the interference on ozone profile retrievals.

In Sect. 2 we briefly introduce satellite measurements of OMI and MLS, used in this study, and then describe PMC detection algorithm and PMC optical depth (POD) retrieval algorithm, respectively. In Sect. 3.1 we evaluate OMI ozone profile retrievals (without POD retrievals) against MLS ozone profiles during the PMC season. Sec-

## Simultaneous Retrievals of PMCs

J. Bak et al.

Title Page

Abstract

Introduction

Conclusions

References

Tables

Figures

◀

▶

◀

▶

Back

Close

Full Screen / Esc

Printer-friendly Version

Interactive Discussion



tion 3.2 presents the results from a retrieval sensitivity study to see if OMI measurements provide adequate sensitivity to measure PMC optical depth. The improvement of ozone profile retrievals with simultaneously retrieved POD is discussed in Sect. 3.3. We summarize and conclude our results in Sect. 4.

## 2 Data and methods

### 2.1 OMI and MLS ozone measurements

Both OMI and MLS instruments are on board the Aura satellite which is flown in a 705 km sun-synchronous polar orbit with ascending equator-crossing time at  $\sim 13:45$ . MLS measurements are taken about 7 min ahead of OMI for the same locations during daytime orbital tracks.

OMI is a nadir-viewing, ultraviolet-visible imaging spectrometer that measures backscattered radiances from 260 to 550 nm (UV-1: 260–310 nm; UV-2: 310–365 nm; VIS: 365–500 nm) at spectral resolutions of 0.42–0.63 nm with daily global coverage. The spatial resolution is 13 km  $\times$  24 km for UV-2 and VIS and 13 km  $\times$  48 km for UV-1 at nadir position in the global mode. The Smithsonian Astrophysical Observatory (SAO) Optimal Estimation (OE)-based ozone profile algorithm (Liu et al., 2010a), is used to retrieve partial column ozone at 24 layers (surface to  $\sim 65$  km) from OMI measurements with the fitting window of 270–330 nm. The a posteriori solution through optimal estimation is given as:

$$\mathbf{X}_{i+1} = \mathbf{X}_i + (\mathbf{K}_i^T \mathbf{S}_y^{-1} \mathbf{K}_i + \mathbf{S}_a^{-1})^{-1} + [\mathbf{K}_i^T \mathbf{S}_y^{-1} (\mathbf{Y} - R(\mathbf{X}_i)) - \mathbf{S}_a^{-1} (\mathbf{X}_i - \mathbf{X}_a)] \quad (1)$$

where  $\mathbf{X}_{i+1}$ ,  $\mathbf{X}_i$ ,  $\mathbf{X}_a$ , and  $\mathbf{Y}$  are the current and previous state vectors, a priori vector, and measured radiance vector (defined as logarithm of normalized radiance), respectively;  $R(\mathbf{X}_i)$  and  $\mathbf{K}_i$  are simulated logarithm of radiance spectrum and the weighting function matrix calculated using the Vector Linearized Discrete Ordinate Radiative

Title Page

Abstract

Introduction

Conclusions

References

Tables

Figures

◀

▶

◀

▶

Back

Close

Full Screen / Esc

Printer-friendly Version

Interactive Discussion



Transfer model (VIDORT) (Spurr, 2006, 2008); the measurement error covariance matrix and a priori covariance matrix are defined as  $\mathbf{S}_y$  and  $\mathbf{S}_a$ , respectively. This iterative process is performed until the cost function  $\chi^2$  (Eq. 2) is converged.

$$\chi^2 = \left\| \mathbf{S}_y^{-\frac{1}{2}} \{K_j(\mathbf{X}_{i+1} - \mathbf{X}_i) - [Y - R(\mathbf{X}_i)]\} \right\|_2^2 + \left\| \mathbf{S}_a^{-\frac{1}{2}} (\mathbf{X}_{i+1} - \mathbf{X}_a) \right\|_2^2. \quad (2)$$

The vertical resolution estimated by Liu et al. (2010a) is  $\sim 7$ – $11$  km in stratosphere. The retrieval precisions range from 1 % in the middle stratosphere to 10 % in the lower stratosphere, the solution errors are typically 1–6 % in the stratosphere

MLS is a forward-looking, thermal-emission, microwave limb sounder that takes measurements along-track and performs 240 limb scans per orbit with a footprint of  $\sim 6$  km across-track and  $\sim 200$  km along-track. The MLS ozone used here is the version 3.3 standard ozone product (55 pressure levels) retrieved from the 240 GHz radiance information, publicly available from the NASA Goddard Space Flight Center Earth Sciences (GES) data and Information Services Center (DISC). The typical vertical resolution of this product is 2.5–3.5 km from 261 to 0.2 hPa and 4–5.5 km from 0.1 to 0.02 hPa (Livesey et al., 2011); the precision is estimated to be a few% in the middle stratosphere, but 5–100 % below 150 hPa and 60–300 % above 0.1 hPa. We apply all the data screening criteria recommended in Livesey et al. (2011) and hence limit MLS ozone data to “quality” higher than 0.6, “convergence” lower than 1.18, positive “precision” values and even “status” value for the pressure range of 261–0.02 hPa.

Liu et al. (2010b) used the v2.2 MLS ozone data to validate the OMI ozone profile retrievals and demonstrated the excellent OMI/MLS agreement within 4 % in the middle stratosphere, except for positive biases of 5–10 % above 0.5 hPa and negative biases of 10–15 % below 100 hPa, which are greatly improved by accounting for OMI’s coarser vertical resolution using OMI averaging kernels.

Simultaneous  
Retrievals of PMCs

J. Bak et al.

Title Page

Abstract

Introduction

Conclusions

References

Tables

Figures



Back

Close

Full Screen / Esc

Printer-friendly Version

Interactive Discussion



## 2.2 OMI PMC detection

The flag data to detect both PMC and non-PMC region from OMI measurements are provided from DeLand et al. (2010). This detection algorithm uses albedo data ( $A = I/F$ ,  $I$  = radiance,  $F$  = irradiance) at 267, 275, 283.5, 287.5, and 292.5 nm after interpolating all spectra to a 0.5 nm grid and averaging three consecutive bins. The PMC pixels are identified using enhancements above the Rayleigh scattering background. The background atmospheric albedo due to Rayleigh scattering and ozone absorption ( $A_{\text{ray}}$ ) is determined using a 4th order fit in solar zenith angle to non-PMC pixels for each orbit, after applying a geometric adjustment for cross-track albedo variations as defined in Eq. (4) of DeLand et al. (2010). Positive signals of albedo residuals ( $A - A_{\text{ray}}$ ) could be induced by “false PMCs” such as random instrument noise and geophysical variability of ozone as well as by PMC scattering. The minimum residual albedo value for PMC detection is derived from measurements of clear atmospheric variability, and is adjusted to eliminate false PMC signal due to instrument noise. The false PMC signal due to a negative ozone deviation is screened out using the wavelength-dependence of PMC signals that become stronger at shorter wavelengths.

## 2.3 PMC optical depth retrievals

In the standard ozone retrieval mode, the atmosphere is divided into 24 layers ( $P_i = 2^{-\frac{i}{2}} \times 1013.15 \text{ hPa}$  for  $i = 0, 23$ ) with the top of atmosphere, layer 24, set at 0.087 hPa ( $\sim 65 \text{ km}$ ). Radiance calculations are made using the VLIDORT model for a Rayleigh atmosphere (no aerosol) assuming Lambertian reflectance for ground surface and for clouds.

Due to the well-defined spatiotemporal range for PMCs, we will first detect PMCs using the PMC detection algorithm specified in Sect. 2.2, and then calculate weighting functions for POD and include them in the state vector with loose constraints. In the POD retrieval mode, we add five more layers between  $\sim 65$  and  $\sim 90 \text{ km}$  ( $P_{29}$ , top of

### Simultaneous Retrievals of PMCs

J. Bak et al.

[Title Page](#)[Abstract](#)[Introduction](#)[Conclusions](#)[References](#)[Tables](#)[Figures](#)[⏪](#)[⏩](#)[◀](#)[▶](#)[Back](#)[Close](#)[Full Screen / Esc](#)[Printer-friendly Version](#)[Interactive Discussion](#)

## Simultaneous Retrievals of PMCs

J. Bak et al.

Title Page

Abstract

Introduction

Conclusions

References

Tables

Figures

◀

▶

◀

▶

Back

Close

Full Screen / Esc

Printer-friendly Version

Interactive Discussion



the atmosphere) at 5 km intervals:  $P_i = 10^{-\left(\frac{(i-24) \times 5 + 65}{16}\right)} \times 1013.15$  for  $i = 25, 29$ . A PMC layer is inserted to the single layer of 80–85 km. Simulating the scattering particles in the radiative process requires the specification of a particle size distribution, the distribution size, and the distribution dispersion width, and a particle shape. The primary component of the PMC particles was first confirmed as non-spherical ice crystals by Hervig et al. (2001). The range of reported radii and size distribution widths is 15–100 nm and 10–20 nm and log-normal or Gaussian size distributions are normally assumed (Englert et al., 2007; Hervig et al., 2009). In this study, PMCs are assumed to be spherical ice particles with a log-normal size distribution ( $r_o = 55$  nm,  $\sigma_g = 1.4$ ), so that Mie theory can be used, because the particle shape plays a minor role in the UV scattering (Baumgarten and Thomas, 2005; Eremenko et al., 2005). The ice refractive index,  $1.33 + 5 \times 10^{-9}i$  at 300 nm from Warren (1984), was used for the entire wavelength range because of low dependence on UV wavelength. The temperature profile is taken from daily National Centers for Environmental Prediction (NCEP) final (FNL) Operational Global analysis data (<http://rda.ucar.edu/datasets/ds083.2/>) below 10 hPa and from climatological data above. We take ozone a priori information from monthly and zonal mean ozone profile climatology presented in McPeters and Labow (2012). Climatological a priori information for PMC optical thickness is not available. It is selected here by trial and error. As a result, the a priori state and its error are set to be and  $10^{-3}$ , respectively. The initial POD value is taken to be  $10^{-4}$ .

### 3 Results and discussion

#### 3.1 OMI/MLS comparison for with/without PMCs

The ozone profile comparisons between OMI without retrieving PMCs and MLS are performed for two polar summer seasons, North Hemisphere (NH), July 2007 and South Hemisphere (SH), January 2008 when PMC occurrence is most frequent in a given year. The comparison is limited to the high-latitude regions 75–85° N and 75–

**Simultaneous  
Retrievals of PMCs**

J. Bak et al.

Title Page

Abstract

Introduction

Conclusions

References

Tables

Figures



Back

Close

Full Screen / Esc

Printer-friendly Version

Interactive Discussion



85° S. The vertical range is limited to altitudes below 0.1 hPa due to the weak vertical ozone information from OMI measurements above. The retrieval is adequately resolved for altitudes below  $\sim 0.5$  hPa in the stratosphere based on the averaging kernels (not shown here). In addition, MLS data have much larger uncertainties at altitudes above 0.1 hPa as mentioned in Sect. 2.1. The collocated OMI and MLS measurements are separated into PMC and non-PMC pixels using the OMI PMC detection flag specified in Sect. 2.2. In order to reduce the effect of OMI smoothing errors on the comparison, the high-resolution MLS data is convolved with OMI averaging kernels. Figure 1 compares the OMI and MLS ozone profiles averaged over PMC and non-PMC regions, respectively, on MLS pressure grids. The mean original/smoothed MLS profiles show no difference due to the presence of PMCs, but the differences become significant for the mean OMI profiles in the upper stratosphere. This demonstrates that the MLS stratospheric ozone product could be a proper reference for the evaluation of impacts of PMCs on OMI ozone retrievals during a PMC season.

Figure 2 shows the mean biases and standard deviations of relative differences between OMI and smoothed MLS ozone profiles. With non-PMC pixels the maximum negative bias of OMI relative to MLS reaches  $-13\%$  for the NH and  $-6\%$  for the SH, respectively, at  $\sim 0.5$  hPa. This bias increases to  $-30\%$  for the NH and  $-24\%$  for the SH when there are PMCs. The mean bias difference between PMC and non-PMC is the difference between the black and green lines in Fig. 1, almost the same as the black line since the MLS PMC/non-PMC difference is almost zero. We can see that the PMC effect on OMI retrievals starts at  $\sim 6$  hPa, leading to erroneous ozone reductions of  $\sim 20\%$  at 0.5 hPa and  $\sim 2\%$  at 2 hPa. This result is generally consistent with the findings of Thomas et al. (1991) that reported the effect of PMCs on SBUV ozone data. However, the comparison of standard deviations shows almost no difference, indicating that the presence of PMCs mainly causes systematic retrieval biases.

In Fig. 3, OMI/MLS biases are plotted as functions of PMC albedo residuals at 267 nm for the NH polar summer (July 2007). This figure emphasizes that brighter PMCs have greater impact on upper atmospheric ozone retrievals from UV measure-



Simultaneous  
Retrievals of PMCs

J. Bak et al.

Title Page

Abstract

Introduction

Conclusions

References

Tables

Figures



Back

Close

Full Screen / Esc

Printer-friendly Version

Interactive Discussion



ments. The OMI-MLS differences increase up to 60–80 % at the topmost three layers when PMCs are very bright. For dark PMC pixels, OMI retrievals agree well with MLS (mean biases are close to zero), except for negative biases of –20 % in 0.15–0.46 hPa and –10 % in 0.68–1.0 hPa. Observations from the Cloud Imaging and Particle Size (CIPS) instrument on the Aeronomy of Ice in the Mesosphere (AIM) satellite show that faint PMCs below the OMI detection threshold, with brightnesses as low as  $1.0 \times 10^{-6} \text{ sr}^{-1}$ , are observed in 80–90 % of all samples at 80° latitude (Lumpe et al., 2013). Thus, even pixels that are “dark” based on the OMI detection threshold may still have enough PMC contamination to bias OMI ozone retrievals above 1.0 hPa. A strong negative correlation of more than 0.5 is found in partial ozone columns above 2 hPa and no correlation ( $< 0.1$ ) at those layers below 6 hPa. Similar behavior is detected for the relationship between biases due to PMCs and albedo residuals in the SH polar summer (January 2008) presented in Table 1.

### 3.2 Sensitivity of UV radiances to PMCs

In Fig. 4a, the sensitivity of OMI radiance to POD ranging from  $10^{-5}$  to  $10^{-3}$  is plotted as functions of wavelength for a Solar Zenith Angle (SZA) of 70°, Viewing Zenith Angle (VZA) of 45° and Azimuth Zenith Angle (AZA) of 135°. Despite being optically thin, PMCs can significantly affect the UV radiances at shorter wavelengths where the signal is weak. The presence of PMCs with the optical depth of  $10^{-3}$  enhances the radiances from 2 % at 300 nm to 8 % at 265 nm for AZA of 135°. This sensitivity increases 4 times for the same SZA and VZA but AZA of 45° (Fig. 4b). Furthermore, it is shown that POD should be larger than  $\sim 10^{-4}$  for the case in Fig. 4a and larger than  $\sim 2 \times 10^{-5}$  in Fig. 4b to be detectable from UV measurements as the OMI measurement errors at  $\sim 270 \text{ nm}$  are  $\sim 1 \%$ .

Figure 4c shows the viewing geometry dependence of PMC sensitivity at 267 nm. The sensitivity varies largely with SZA, VZA, and AZA, except that at AZA larger than 90° the dependence on viewing geometry becomes relatively insignificant. This dependence on AZA is mainly due to the steeper phase function variation of PMCs at forward

scattering angles, displayed in Fig. 4d. The significant increase in PMC sensitivity with larger SZA or VZA at AZA < 90° is mainly due to the larger photon path length for PMC scattering. Overall, the dependence on viewing geometry is a direct result of the strength of the PMC scattering.

Sensitivity studies using the optimal estimation formulation (with a loose PMC a priori constraint of 10<sup>-3</sup>) show that POD can be retrieved with errors from 1–6.5 × 10<sup>-4</sup> depending on viewing geometry, as shown in Fig. 5. The POD retrieval errors are smaller at longer slant paths and smaller AZAs where the scattering is stronger and sensitivity becomes larger. The typical AZA for OMI PMC detection varies from 40 to 130° (SZAs > 40°, latitude > 60° N/S) so the errors of OMI POD retrievals are expected to have significant dependence on the scattering angle.

Figure 6 shows the impact of PMCs on ozone profile retrievals due to the neglect of PMCs, estimated as  $\frac{\partial \widehat{x_{O3}}}{\partial Y} \cdot \frac{\partial Y}{x_{POD}} \cdot \Delta \text{POD}$ . This result is generally consistent with the effect of PMCs on the OMI and MLS comparisons shown in Figs. 1 and 2: The presence of PMCs results in negative ozone retrieval errors above 6 hPa, the ozone errors increase rapidly up to ~ 0.5 hPa and continue to increase with the greatest peak impact at 0.2 hPa (60 km). At AZA = 135° (Fig. 6a) ozone errors increase -2.5 % for POD of 10<sup>-4</sup> to -25 % for POD of 10<sup>-3</sup>. These ozone retrieval errors are expected to increase at longer slant paths and smaller AZAs. For example, as shown in Fig. 6b, the errors increase by a factor of 5 when the AZA is changed to 45°.

### 3.3 Simultaneous retrievals of ozone profile and PMC optical depth

As mentioned in Sect. 2.3, the POD a priori value and its error are determined as 0 and 10<sup>-3</sup>, respectively, by trial and error. The POD initial value of 10<sup>-4</sup> is close to the minimum value that is detectable from BUUV radiances below 300 nm as shown in Fig. 4. An example for POD retrieved from OMI nadir measurements with three a priori errors is presented in Fig. 7. This example illustrates that the a priori error value of 10<sup>-4</sup> is a very tight constraint as the retrieved POD values are very small for both PMC and

Title Page

Abstract

Introduction

Conclusions

References

Tables

Figures



Back

Close

Full Screen / Esc

Printer-friendly Version

Interactive Discussion



## Simultaneous Retrievals of PMCs

J. Bak et al.

Title Page

Abstract

Introduction

Conclusions

References

Tables

Figures



Back

Close

Full Screen / Esc

Printer-friendly Version

Interactive Discussion



non-PMC pixels. This also indicates that the POD can be consistently retrieved from measurement information with a priori error values  $\geq 10^{-3}$ , implying that the degree of freedom for signal is close to 1 for the POD parameter. The retrieved optical depths are generally larger at PMC pixels than at non-PMC pixels. Furthermore, the significant correlation ( $r = \sim 0.8$ ) between POD and albedo residuals is demonstrated in Fig. 8. The typical value of the retrieved optical depth is around  $1\text{--}5 \times 10^{-4}$  and increases up to  $15 \times 10^{-4}$  for bright PMC pixels. Solution errors for PMC increase from  $1 \times 10^{-4}$  at larger SZAs to  $4 \times 10^{-4}$  at smaller SZAs. These retrieval errors are distinctly smaller than the a priori error of  $10^{-3}$ . This result are consistent with the sensitivity studies as shown in Fig. 5, considering the AZAs for OMI measurements used in Fig. 7 vary from 61 and 89° and VZAs are within 11°.

Figure 8b compares the retrieved ozone columns above 40 km with and without including the POD in the state vector. It illustrates that the ozone values become larger when the PODs are simultaneously retrieved. The ozone column differences are larger for PMC pixels than for non-PMC pixels, indicating that the simultaneously retrieved POD could correct the negative biases in OMI ozone retrievals. Figures 9 and 10 evaluate the improvements of OMI/MLS ozone profile comparisons with the simultaneous retrievals of POD and ozone. The systematic biases due to PMCs are mostly corrected, especially for bright PMC pixels: the negative biases range from 15 to 50% depending on the PMC albedo residuals in the upper atmosphere, but are reduced to within  $\pm 10\%$  below 1–2 hPa. The significant negative correlation between OMI/MLS ozone differences and PMC albedo residuals found in Fig. 3 is reduced to within 0.1 in most layers, except for the topmost two layers ( $R = -0.25$ ). However, the simultaneous ozone/POD retrievals systematically show positive biases ( $\sim 10\%$ ) for the layers of 1.21–2.15 hPa relative to MLS data, irrespective of albedo residuals, and even for non-PMC pixels.

## 4 Conclusions

This work demonstrated the interference of tenuous PMCs on OMI ozone profile retrievals above 6 hPa. The presence of PMCs leads to the systematic biases of  $-2\%$  at 2 hPa and  $-20\%$  at 0.5 hPa in OMI-MLS differences. The magnitude of OMI/MLS differences can increase to up to  $\sim 60\text{--}80\%$  for very bright PMC pixels. Sensitivity analysis shows that the PMC sensitivity is strongly dependent on wavelength, larger at shorter wavelengths where the signals are weak. PMC sensitivity is also strongly dependent on viewing geometry in the forward scattering direction (e.g., relative azimuth angles less than  $90^\circ$ ); PMC sensitivity increases with larger SZAs and VZAs due to longer path lengths for PMC scattering and especially with smaller AZAs due to much stronger forward scattering. For AZAs greater than  $90^\circ$ , the dependence becomes insignificant because the PMC scattering varies much less with viewing geometry. PMC optical depth of  $\sim 10^{-4}$  is detectable from OMI data in the back scattering direction and the PMC detection limit could be smaller for the forward scattering direction. The maximum contribution of ignoring PMC to ozone retrievals is found at  $\sim 0.2$  hPa. To reduce PMC interference on ozone retrievals, we added the PMC optical depth (POD) to the state vector in OMI optimal estimation ozone profile algorithm. The PMC a priori value and a priori error are set at 0 and  $10^{-3}$ , respectively in this study. The selected a priori error value corresponds to a loose constraint, implying that the retrieved optical depth comes mainly from measurement information. As a result, the POD can be retrieved with uncertainties of  $1\text{--}4 \times 10^{-4}$  depending on solar zenith angles. A near-linear relationship is found between POD and albedo residuals ( $R \sim 0.8$ ); the retrieved POD values are  $1\text{--}5 \times 10^{-4}$  at dark PMC pixels and increase up to  $15 \times 10^{-4}$  for bright PMC pixels. It is demonstrated that the simultaneous retrieval of POD could improve the OMI and MLS comparisons. The negative OMI biases are reduced to within  $\pm 10\%$  after simultaneous ozone/POD retrievals. In addition, this simultaneous retrieval reduces the strong negative correlation between OMI/MLS biases and PMC albedo residuals to  $\sim 0.1$  above 2 hPa, which is found to be stronger than  $-0.5$  for ozone retrieval only.

## Simultaneous Retrievals of PMCs

J. Bak et al.

Title Page

Abstract

Introduction

Conclusions

References

Tables

Figures



Back

Close

Full Screen / Esc

Printer-friendly Version

Interactive Discussion



*Acknowledgements.* The authors would like to thank OMI and MLS science teams for providing the satellite data. Research at Pusan National University by J. Bak and J. H. Kim was supported by the Eco Innovation Program of KEITI (ARQ201204015), South Korea. Research at the Smithsonian Astrophysical Observatory by X. Liu, K. Chance as well as J. Bak during her 3 month visit to Harvard-Smithsonian was funded by NASA and the Smithsonian Institution.

## References

- Baumgarten, G. and Thomas, G. E.: The importance of ice particle shape on UV measurements of polar mesospheric clouds: SBUV/2 observations, *J. Atmos. Sol.-Terr. Phys.*, 68, 78–84, doi:10.1016/j.jastp.2005.08.007, 2006.
- DeLand, M. T. and Thomas, G. E.: Updated PMC trends derived from SBUV data, *J. Geophys. Res.-Atmos.*, 120, 2140–2166, doi:10.1002/2014JD022253, 2015.
- DeLand, M. T., Shettle, E. P., Thomas, G. E., and Olivero, J. J.: Solar backscattered ultraviolet (SBUV) observations of polar mesospheric clouds (PMCs) over two solar cycles, *J. Geophys. Res.*, 108, 8445, doi:10.1029/2002JD002398, 2003.
- DeLand, M. T., Shettle, E. P., Thomas, G. E., and Olivero, J. J.: Latitude-dependent long-term variations in polar mesospheric clouds from SBUV version 3 PMC data, *J. Geophys. Res.*, 112, D10315, doi:10.1029/2006JD007857, 2007.
- DeLand, M. T., Shettle, E. P., Levelt, P. F., and Kowalewski, M. G.: Polar Mesospheric Clouds (PMCs) observed by the Ozone Monitoring Instrument (OMI) on Aura, *J. Geophys. Res.*, 115, D21301, doi:10.1029/2009JD013685, 2010.
- Englert, C. R. and Stevens, M. H.: Polar mesospheric cloud mass and the ice budget: 1. Quantitative interpretation of mid-UV cloud brightness observations, *J. Geophys. Res.*, 112, 08204, doi:10.1029/2006JD007533, 2007.
- Eremenko, M. N., Petelina, S. V., Zasetsky, A. Y., Karlsson, B., Rinsland, C. P., Llewellyn, E. J., and Sloan, J. J.: Shape and composition of PMC particles derived from satellite remote sensing measurements, *Geophys. Res. Lett.*, 32, L16S06, doi:10.1029/2005GL023013, 2005.

Simultaneous  
Retrievals of PMCs

J. Bak et al.

Title Page

Abstract

Introduction

Conclusions

References

Tables

Figures



Back

Close

Full Screen / Esc

Printer-friendly Version

Interactive Discussion



Hervig, M., Thompson, R. E., McHugh, M., Gordley, L. L., Russell III, J. M., and Summers, M. E.: First confirmation that water ice is the primary component of polar mesospheric clouds, *Geophys. Res. Lett.*, 28, 971–974, 2001.

Hervig, M. E., Gordley, L. L., Stevens, M. H., Russell III, J. M., Bailey, S. M., and Baumgarten, G.: Interpretation of SOFIE PMC measurements: cloud identification and derivation of mass density, particle shape, and particle size, *J. Atmos. Sol.-Terr. Phys.*, 71, 316–330, 2009.

Liu, X., Bhartia, P. K., Chance, K., Spurr, R. J. D., and Kurosu, T. P.: Ozone profile retrievals from the Ozone Monitoring Instrument, *Atmos. Chem. Phys.*, 10, 2521–2537, doi:10.5194/acp-10-2521-2010, 2010a.

Liu, X., Bhartia, P. K., Chance, K., Froidevaux, L., Spurr, R. J. D., and Kurosu, T. P.: Validation of Ozone Monitoring Instrument (OMI) ozone profiles and stratospheric ozone columns with Microwave Limb Sounder (MLS) measurements, *Atmos. Chem. Phys.*, 10, 2539–2549, doi:10.5194/acp-10-2539-2010, 2010b.

Livesey, N. J., Read, W. G., Froidevaux, L., Lambert, A., Manney, G. L., Pumphrey, H. C., Santee, M. L., Schwartz, M. J., Wang, S., Cofeld, R. E., Cuddy, D. T., Fuller, R. A., Jamot, R. F., Jiang, J. H., Knosp, B. W., Stek, P. C., Wagner, P. A., and Wu, D. L.: Version 3.3 Level 2 data quality and description document, JPL California Institute of Technology, Pasadena, CA 91109-8099, 2011.

Lumpe, J. D., Bailey, S. M., Carstens, J. N., Randall, C. E., Rusch, D. W., Thomas, G. E., Nielsen, K., Jeppesen, C., McClintock, W. E., Merkel, A. W., Riesberg, L., Templeman, B., Baumgarten, G., and Russell III, J. M.: Retrieval of polar mesospheric cloud properties from CIPS: algorithm description, error analysis and cloud detection sensitivity, *J. Atmos. Sol-Terr. Phys.*, 104, 167–196, 2013.

McPeters, R. D. and Labow, G. J.: Climatology 2011: an MLS and sonde derived ozone climatology for satellite retrieval algorithms, *J. Geophys. Res.*, 1117, 10303, doi:10.1029/2011JD017006, 2012.

Shettle, E. P., DeLand, M. T., Thomas, G. E., and Olivero, J. J.: Long term variations in the frequency of polar mesospheric clouds in the Northern Hemisphere from SBUV, *Geophys. Res. Lett.*, 36, 02803, doi:10.1029/2008GL036048, 2009.

Taylor, M. J., Gadsden, M., Lowe, R. P., Zalcik, M. S., and Brausch, J.: Mesospheric cloud observations at unusually low latitudes, *J. Atmos. Sol. Terr. Phys.*, 64, 991–999, 2002.

Thomas, G. E., McPeters, R. D., and Jensen, E. J.: Satellite observations of polar mesospheric clouds by the solar backscattered ultraviolet spectral radiometer – evidence of a solar cycle dependence, *J. Geophys. Res.*, 96, 927–939, 1991.

Warren, S. G.: Optical constants of ice from the ultraviolet to the microwave, *Appl. Optics*, 23, 1206–1225, doi:10.1364/AO.23.001206, 1984.

5

Simultaneous Retrievals of PMCs

J. Bak et al.

Title Page

Abstract

Introduction

Conclusions

References

Tables

Figures



Back

Close

Full Screen / Esc

Printer-friendly Version

Interactive Discussion



## Simultaneous Retrievals of PMCs

J. Bak et al.

Title Page

Abstract

Introduction

Conclusions

References

Tables

Figures



Back

Close

Full Screen / Esc

Printer-friendly Version

Interactive Discussion



**Table 1.** Correlation between OMI/convolved MLS ozone difference and PMC albedo residual at 267 nm as shown in Fig. 3, but for SH 2008 summer.

Layer (hPa)	Correlation	Layer (hPa)	Correlation
0.15–0.22	–0.42	1.78–2.15	–0.49
0.32–0.46	–0.57	2.61–3.16	–0.36
0.68–1.00	–0.59	3.83–4.64	–0.27
1.21–1.47	–0.54	5.62–6.81	–0.14



Simultaneous  
Retrievals of PMCs

J. Bak et al.

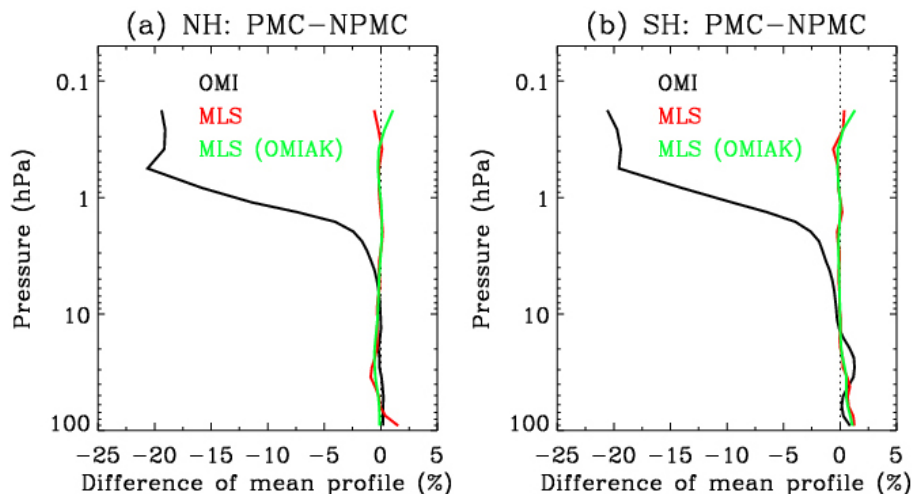


**Figure 1.** Difference of mean ozone profiles from OMI (black), collocated MLS (red), and MLS convolved with OMI averaging kernels (green) between PMC and non-PMC pixels ( $(\text{PMC} - \text{NPMC}/\text{NPMC}) \times 100\%$ ). **(a)** and **(b)** are results from NH 2007 (July 2007, 75–85° N) and SH 2008 (January 2008, 75–85° S) summer seasons, respectively.

Simultaneous  
Retrievals of PMCs

J. Bak et al.

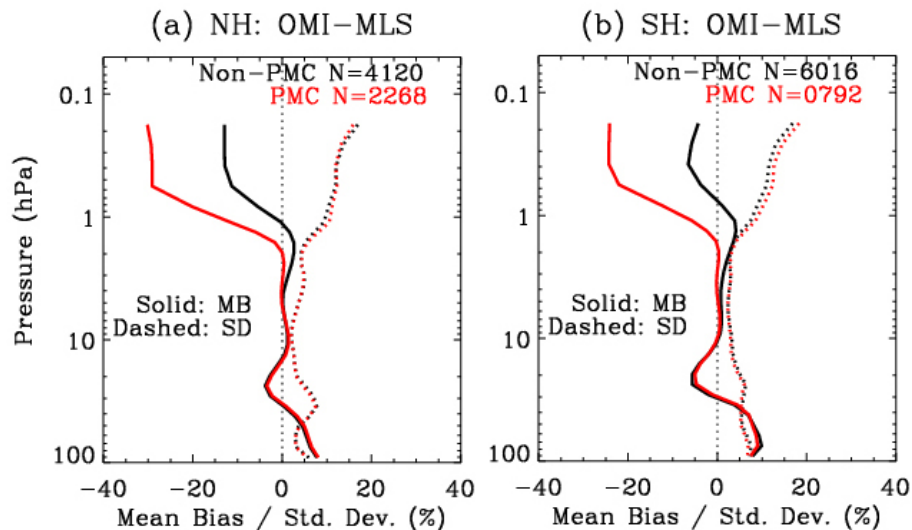


**Figure 2.** Collocated OMI/convolved MLS differences,  $(\text{OMI} - \text{MLS})/\text{OMI}$  a priori  $\times 100\%$ , (solid lines) and their  $1\sigma$  standard deviations (dashed lines) for PMC (red) and non-PMC (black) pixels for both hemispheric polar summer seasons, respectively.

Title Page

Abstract

Introduction

Conclusions

References

Tables

Figures

◀

▶

◀

▶

Back

Close

Full Screen / Esc

Printer-friendly Version

Interactive Discussion



## Simultaneous Retrievals of PMCs

J. Bak et al.

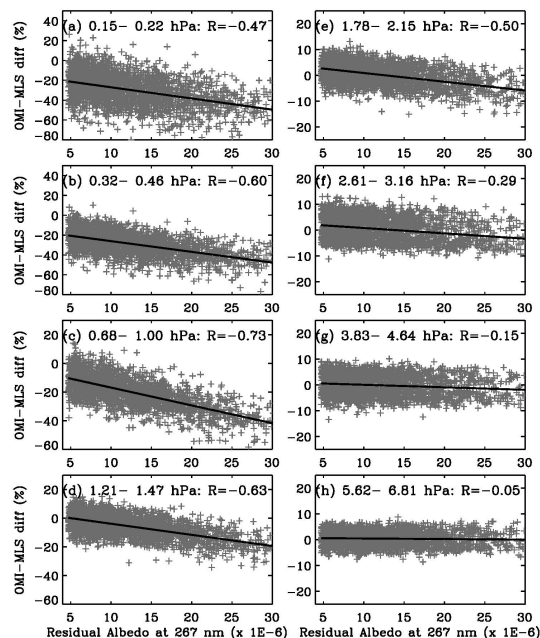


**Figure 3.** Scatter plots between OMI/convolved MLS partial column ozone difference (%) for eight MLS layers and PMC albedo residual at 267 nm for NH 2007 summer. The correlation coefficients ( $R$ ) are shown in the legend.

Title Page

Abstract

Introduction

Conclusions

References

Tables

Figures



Back

Close

Full Screen / Esc

Printer-friendly Version

Interactive Discussion



Simultaneous  
Retrievals of PMCs

J. Bak et al.

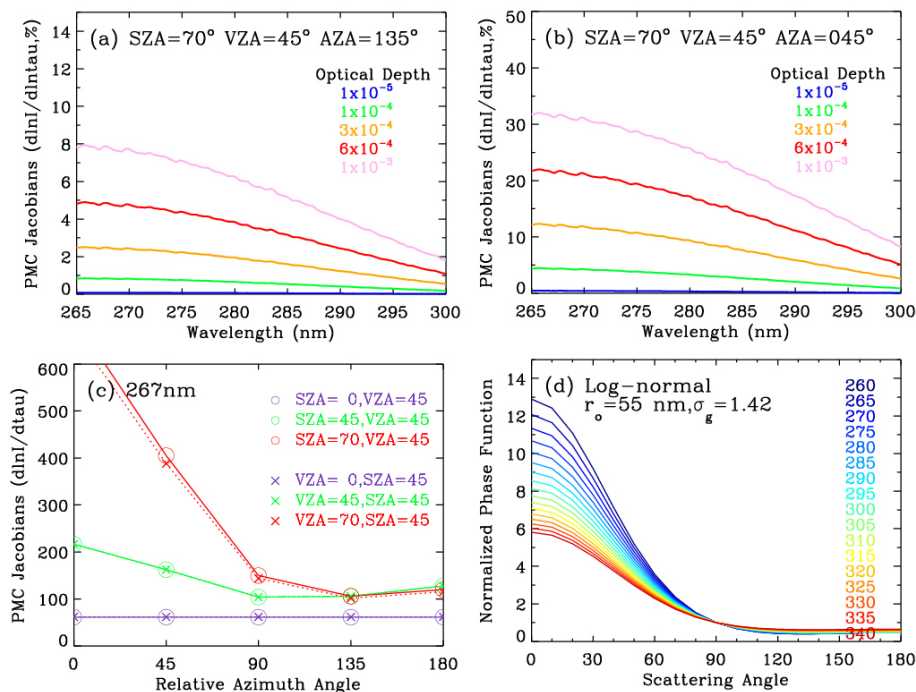


**Figure 4.** (a) Jacobians with respect to PMC optical depth (“ $\tau$ ”) as functions of wavelength at  $SAZ = 70^\circ$ ,  $VZA = 45^\circ$ , and  $AZA = 135^\circ$  for five optical depth values ranging from  $10^{-5}$  to  $10^{-3}$ . (b) Same as (a), but for  $AZA = 45^\circ$ . (c) Normalized PMC Jacobians at 267 nm as a function of AZA with various  $SAZ$ s and  $VZA$ s. (d) PMC phase function as a function of scattering angle ( $\Phi$ ) for wavelengths ranging from 260 to 340 nm, normalized to unity at  $\Phi = 90^\circ$ .

Title Page

Abstract

Introduction

Conclusions

References

Tables

Figures



Back

Close

Full Screen / Esc

Printer-friendly Version

Interactive Discussion



## Simultaneous Retrievals of PMCs

J. Bak et al.

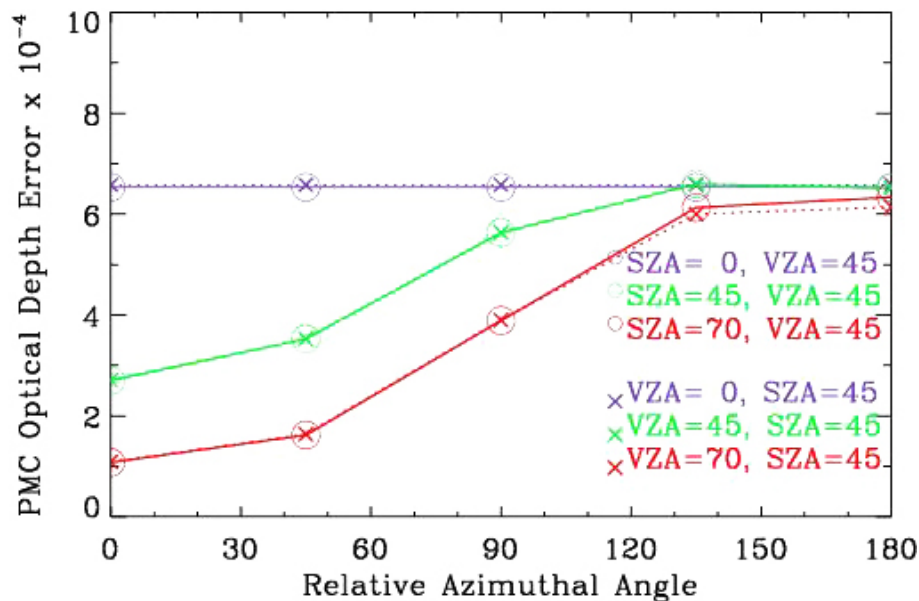


**Figure 5.** Same as Fig. 4c, but for PMC optical depth retrieval errors (root sum square of random-noise and smoothing errors).

Title Page

Abstract

Introduction

Conclusions

References

Tables

Figures

◀

▶

◀

▶

Back

Close

Full Screen / Esc

Printer-friendly Version

Interactive Discussion



Simultaneous  
Retrievals of PMCs

J. Bak et al.

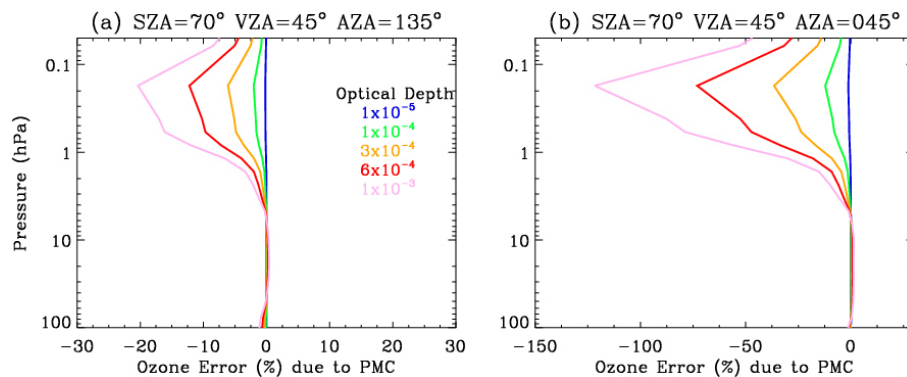


**Figure 6.** Ozone profile retrieval errors as functions of pressure due to the neglect of PMCs estimated based on the optimal estimation approach.

[Title Page](#)[Abstract](#)[Introduction](#)[Conclusions](#)[References](#)[Tables](#)[Figures](#)[◀](#)[▶](#)[◀](#)[▶](#)[Back](#)[Close](#)[Full Screen / Esc](#)[Printer-friendly Version](#)[Interactive Discussion](#)

## Simultaneous Retrievals of PMCs

J. Bak et al.

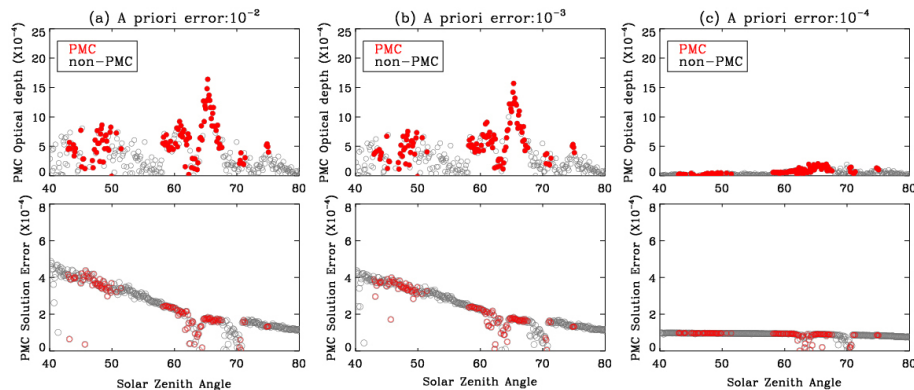


**Figure 7.** Retrieved PMC optical depth values and retrieval errors as functions of solar zenith angle for OMI orbit number 15881 and cross-track position 13 (UV1) with a fixed a priori value of 0 and three a priori error values, **(a)**  $10^{-2}$ , **(b)**  $10^{-3}$  and **(c)**  $10^{-4}$ , respectively.

Title Page

Abstract

Introduction

Conclusions

References

Tables

Figures



Back

Close

Full Screen / Esc

Printer-friendly Version

Interactive Discussion



Simultaneous  
Retrievals of PMCs

J. Bak et al.

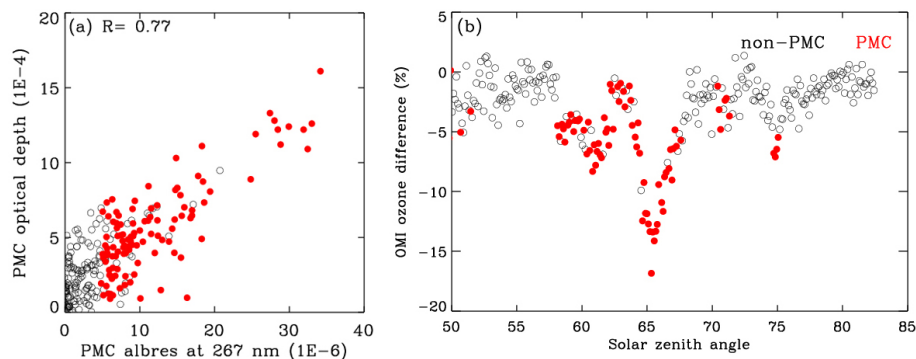


**Figure 8.** (a) Scatter plot between retrieved PMC optical depths (POD) and PMC albedo residuals at 267 nm for OMI orbit number 15 881 and cross-track position 13 (UV1). (b) OMI ozone column (above 40 km) differences between “ozone only” and “ozone + POD” retrieval modes.

[Title Page](#)[Abstract](#)[Introduction](#)[Conclusions](#)[References](#)[Tables](#)[Figures](#)[◀](#)[▶](#)[◀](#)[▶](#)[Back](#)[Close](#)[Full Screen / Esc](#)[Printer-friendly Version](#)[Interactive Discussion](#)



## Simultaneous Retrievals of PMCs

J. Bak et al.

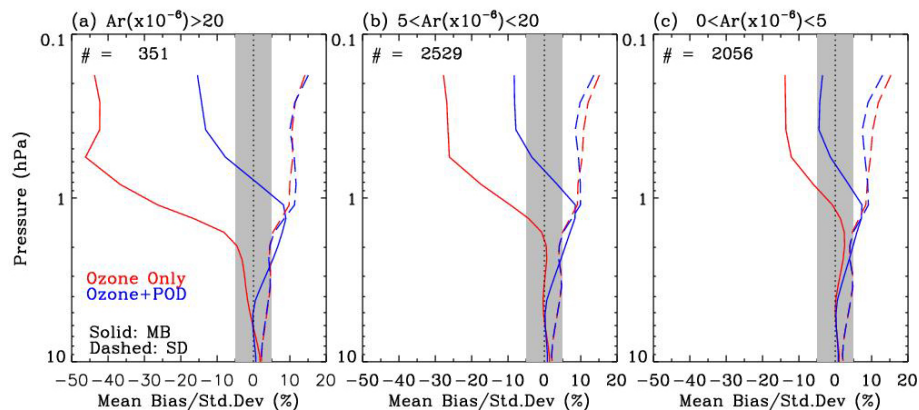


**Figure 9.** Collocated OMI/convolved MLS profile differences (solid lines) and their  $1\sigma$  standard deviations (dashed lines) for different ranges of PMC albedo residual ( $Ar$ ) values at 267 nm for the NH 2007 summer season. Note that the number of the PMC pixels is 314, 1876, 61, respectively. The blue and red lines represent the comparisons when OMI ozone profiles are retrieved with and without PMC optical depths (PODs), respectively.

Title Page

Abstract

Introduction

Conclusions

References

Tables

Figures

◀

▶

◀

▶

Back

Close

Full Screen / Esc

Printer-friendly Version

Interactive Discussion



## Simultaneous Retrievals of PMCs

J. Bak et al.

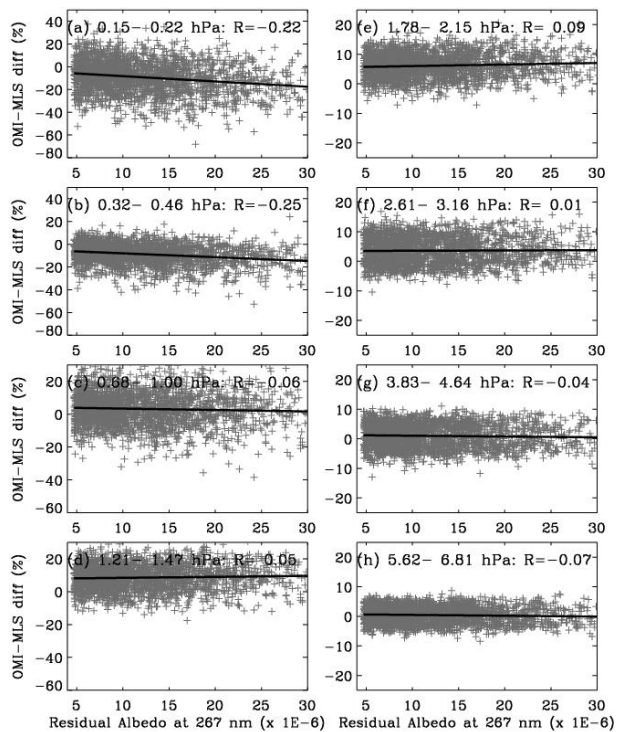


**Figure 10.** Same as Fig. 3, but with PMC optical depths simultaneously retrieved with ozone.

Title Page

Abstract

Introduction

Conclusions

References

Tables

Figures



Back

Close

Full Screen / Esc

Printer-friendly Version

Interactive Discussion

